Modelling macroseismic observations for historical earthquakes: the cases of the M = 7.0, 1954 Sofades and M = 6.8, 1957 Velestino events (central Greece)

Giannis Papazachos, Costas Papazachos, Andreas Skarlatoudis, Harris Kkallas & Efthimios Lekkas

Journal of Seismology

ISSN 1383-4649
Volume 20
Number 1

J Seismol (2016) 20:151-165
DOI 10.1007/s10950-015-9517-9

Springer

J Seismol (2016) 20:151–165
DOI 10.1007/s10950-015-9517-9

ORIGINAL ARTICLE

Modelling macroseismic observations for historical earthquakes: the cases of the $M = 7.0$, 1954 Sofades and $M = 6.8$, 1957 Velestino events (central Greece)

Giannis Papazachos · Costas Papazachos · Andreas Skarlatoudis · Harris Kkallas · Efthimios Lekkas

Received: 4 February 2015 / Accepted: 7 August 2015 / Published online: 26 August 2015

Abstract We attempt to model the spatial distribution of the strong ground motion for the large $M = 7.0$, 1954 Sofades and $M = 6.8$, 1957 Velestino events (southern Thessaly basin, central Greece), using the macroseismic intensities (I_{MM} up to 9+) observed within the broader Thessaly area. For this reason, we employ a modified stochastic method realised by the EXSIM algorithm for extended sources, in order to reproduce the damage distribution of these earthquakes, in an attempt to combine existing earthquake information and appropriate scaling relations with surface geology and to investigate the efficiency of the available macroseismic data. For site-effects assessment, we use a new digital geological map of the broader Thessaly basin, where geological formations are grouped by age and mapped on appropriate NEHRP soil classes. Using the previous approach, we estimate synthetic time series for different rupture scenarios and employ various calibrating relations between PGA/PGV and macroseismic intensity, allowing the generation of synthetic (stochastic) isoseismals. Also, different site amplification factors proposed for the broader Aegean area, according to local geology, are tested. Finally, we also perform a sensitivity analysis of the fault location, taking into account the available neotectonic data for the broader southern Thessaly fault zone. The finally determined fault locations are different than previously proposed, in agreement with the available neotectonic information. The observed macroseismic intensities are in good agreement with the ones derived from the synthetic waveforms, verifying both the usefulness of the approach, as well as of the macroseismic data used. Finally, site-effects show clear correlation with the geological classification employed, with constant amplification factors for each soil class generally providing better results than generic transfer functions.

Keywords Macroseismic observations · Stochastic simulation · EXSIM · Thessaly basin · Southern Thessaly fault zone · Historical earthquakes · Site-effects

G. Papazachos (✉) · E. Lekkas
Faculty of Geology & Geoenvironment, National & Kapodistrian University of Athens, Panepistimioupoli Zografou, GR15784, Athens, Greece
e-mail: jpapazahos@gmail.com

C. Papazachos · A. Skarlatoudis · H. Kkallas
Geophysical Laboratory, Aristotle University of Thessaloniki, PO Box 352-1, GR54124, Thessaloniki, Greece

1 Introduction

Thessaly is located in the back-arc Aegean microplate area and is one of the most seismically active regions of Greece. The area has been shown to expand

in a more-or-less N-S direction (see Fig. 1), with a velocity of ∼1 cm/year, due to the active stress field. The result of this extension is the creation of normal faults mainly along its southern and northern borders, with dominant east-west strikes, which dip towards the north (along the southern Thessaly fault zone) or the south (mostly in the northern Thessaly area, Caputo and Pavlides 1993; Mountrakis et al. 1993; Papazachos and Papazachou 2002). This dominant E-W faulting pattern is also found along the western Thessaly border, where it co-exists with the N-S normal faults of the Hellenides mountain belt (e.g. Lekkas 1987).

The Thessaly basin, the largest basin in central Greece, has a well-known history of large earthquakes, with mainshocks having typical moment magnitudes between 6.0 and 7.0 (we have employed moment magnitudes for all processing and figures throughout this study). The seismicity (both instrumental and historic) follows the two discrete rupture zones of the Thessaly basin (e.g. Papazachos et al. 1993), also presented in Fig. 1. The northern rupture zone, along Peneus River, is formed by relatively small faults (typically <25 km), associated mainly with historical earthquakes with magnitudes up to ∼6.5. In the southern Thessaly zone, along the boundaries of the Thessaly plain, the faults are relatively large (up to ∼50 km), associated with earthquakes exhibiting maximum magnitudes up to M∼7.0. During the twentieth century, eight major seismic sequences with mainshock magnitudes equal or larger than 6.0 occurred in this area (1905, 1911, 1930, 1941, 1954, 1955, 1957, 1980), with the M = 7.0, 1954 Sofades earthquake (April 30, 39.28° N, 22.29° E, see Fig. 2) being the largest event. The available descriptions for this event (Papastamatiou and Mouyaris 1986; Papazachos and Papazachou 2002) report damages in the prefectures of Karditsa, Larisa, Trikala, Phthiotida, Magnesia and Evritania. Overall, 6599 buildings were destroyed, 9154 were heavily damaged, 12920 were slightly damaged, while the town of Sofades, in the Karditsa prefecture, was severely damaged. In total, 25 people were killed and 157 were injured. Also, ground fissures, liquefaction phenomena and hydrological changes were observed in several places. The largest foreshock (M = 4.6) occurred on April 25 and the largest aftershock (M = 5.7) on May 4. The 1954 event marked the beginning of a series of earthquakes along the southern Thessaly rupture zone, which also involved the 1955 and 1957 events (Papastamatiou and Mouyaris 1986). The available descriptions for the M = 6.8, 1957 Velestino earthquake (March 8, 39.38° N, 22.63° E, see Fig. 3), given by Papazachos and Papazachou (2002), report serious damages in the prefectures of Magnesia, Larissa, Karditsa and Trikala. A total of 32701 buildings were damaged, 6934 of which collapsed, 10847 were seriously damaged and 14920 were lightly damaged. Two people were killed while 71 were injured. A large foreshock (M = 6.5) occurred a few minutes before the mainshock and its consequences cannot be distinguished from those of the mainshock. The largest aftershock (M = 6.0) occurred several hours after the mainshock.

In the present work, we attempt to simulate the damage distribution for the 1954, M = 7.0 Sofades earthquake, as well as the M=6.8, 1957 Velestino earthquake, using simulated seismic motions. These motions are appropriately converted to macroseismic intensity, after incorporating the site-effect through the local geology. For this reason, we have applied the stochastic simulation method, which has been efficiently used for strong-motion simulation applications during the last three decades.

The stochastic simulation method was initially proposed by Boore (1983) as a point-source method and then applied by many researchers, in order to simulate the ground motion from seismic sources (e.g. Boore and Atkinson 1987; Toro and MacGuire 1987; Ou and Hermann 1990; Atkinson and Boore 1995; Zonno et al. 2010). EXSIM is a modified stochastic simulation algorithm, using finite-fault modelling with a dynamic corner frequency approach (Motazedian and Atkinson 2005). In the present work, we have used EXSIM as adapted by Boore (2009), in order to generate synthetic time series for selected earthquake fault rupture scenarios and estimate peak ground acceleration (PGA) and peak ground velocity (PGV) from the synthetic time series. The main advantage of the proposed approach is that it can reproduce realistic strong motion intensity measures (e.g. PGA, PSA, etc.), although the modelled ruptures are specified by a few simple metrics, such as earthquake magnitude and distance, with options to include more detailed information on fault geometry and slip. In EXSIM, the fault is divided into equal sized subfaults, considered as point sources. The ground motions are calculated for

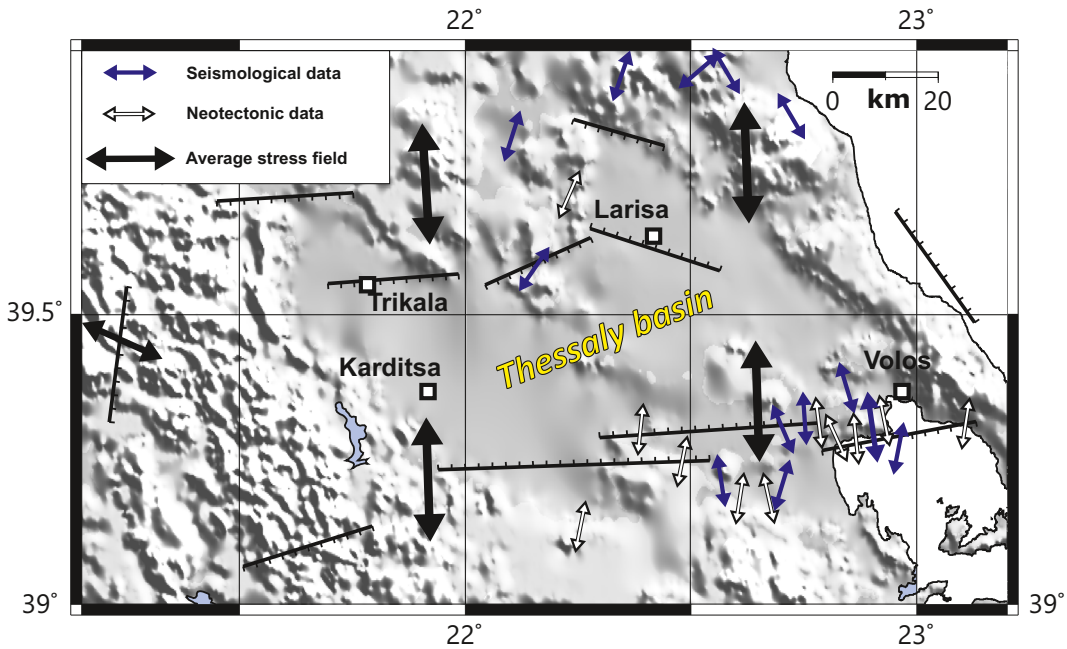

Fig. 1 N-S extensional stress field in the Thessaly basin, and the associated major active E-W striking faults (adopted from Papazachos et al. 2001). Small arrows denote T-axes from neotectonic and earthquake observations, while large arrows depict the average stress field of the study area (modified from Panagiotopoulos and Papazachos 2008)

each subfault using the original point-source method and then summed at the observation point. In most cases, a random rupture scenario can be considered in the simulations, though it is possible to introduce specific rupture scenarios (e.g. bi-directional, etc.)

To assess the effect of the local site conditions on seismic motions, it is clear that detailed geophysical or geotechnical information could not be employed, due to the scale of the study area. For this reason, we relied on the available geological information, which can provide an initial base for site-effect characterisation. Geological formations were hand-digitized using the available Greek Institute of Geology and Mineral Exploration (IGME) maps (scale 1:50000) and then clustered according to their age, hence their expected dynamic amplification behaviour, into the following four classes (also see Fig. 2):

1. Bedrock/Basement rocks (Mesozoic-Paleogene age)
2. Molassic type sediments (Paleogene-Neogene age)
3. Neogene sediments
4. Quaternary-Plio/Pleistocene sediments

2 Simulation of the 1954 Sofades earthquake

2.1 Generating synthetic macroseismic maps with stochastic simulation

Macroseismic data were collected from the published database of macroseismic information for the Aegean area (Papazachos et al. 1997). Observed intensities, ranging from $I_{MM} = 5$ to $I_{MM} = 9+$, were available for 75 settlements. The locations of these settlements were used as target sites for the simulations. Overall, 19 of the simulation target sites fall into geological class 1, 4 fall into class 2 and 52 fall into class 4.

The fault location was initially constrained following the focal parameters (hypocentre and fault location, fault strike and dip, faulting type, etc.) provided by Papazachos et al. (2001). The fault's dimensions (length, L, and width, w) were estimated using the following Eqs. 1 and 2:

$$log_{10}L = 0.50M - 1.86 \quad (1)$$

$$log_{10}w = 0.28M - 0.70 \quad (2)$$

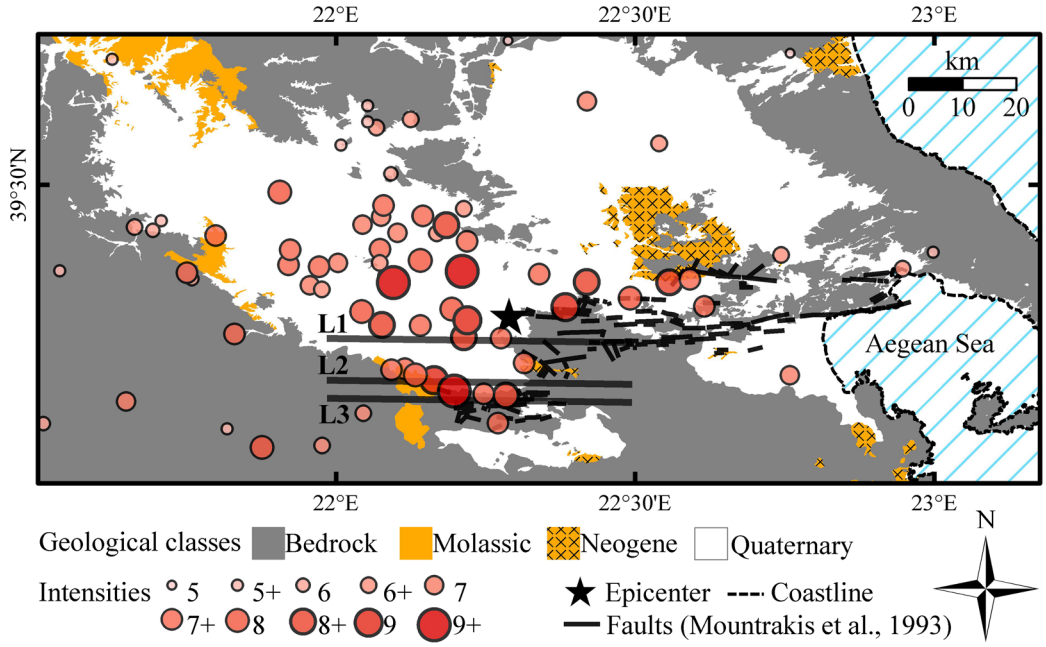

Fig. 2 Observed macroseismic intensities (Modified Mercalli scale), catalogue epicentre of the M = 7.0, 1954 Sofades earthquake, and main geological formation classes within the broader Thessaly basin area. The three candidate locations for the upper Sofades fault edge (L1–L3) considered in the present study for the 1954 event, as well as the main active faults in southern Thessaly, proposed by Mountrakis et al. (1993), are also presented

which have been proposed for the estimation of earthquake fault dimensions from moment magnitude for continental dip-slip faults (Papazachos et al. 2004; Papazachos et al. 2006). The dimensions (length, ΔL and width, Δw) of each subfault were constrained from Eq. 3, proposed by Beresnev and Atkinson 1999:

$$log_{10}\Delta l = -2 + 0.4M \quad (3)$$

and were slightly modified in order to match the calculated fault dimensions. The available field observations (Papastamatiou and Mouyaris 1986; Mountrakis et al. 1993) showed a large number of surface fissures and very small surface rupture segments, without revealing a clear surface manifestation of the seismic fault along its length. For this reason, the depth of the upper edge of the fault was set to 1 km, close to the surface. The sensitivity analysis performed for this parameter showed that larger depths resulted in systematic underestimation of macroseismic intensities, suggesting that the adopted depth choice was appropriate.

For the simulation, the stress parameter was set to 70 bars (Boore and Joyner 1997). The value 56 bars which has been proposed for normal and strike-slip faults in Greece by Margaris and Boore (1998) and is based on a relatively small number of data, was also tested, but did not have significant impact on the resulting ground motion levels, hence its effect could not be resolved, at least using the available macroseismic information. The crust's average shear wave velocity (β) and density (ρ) were derived from Papazachos et al. (1966). The rupture propagation velocity, V_{rup}, was set at a typical value of 0.8. Larger values (V_{rup} = 0.9 and 0.95) were also tested, resulting in slightly lower (underestimated) synthetic macroseismic values for the southern Thessaly observation sites for the higher V_{rup} value. Different values were used for the high-frequency attenuation parameter, κ, according to the geology/soil class of each simulation site, as shown in Table 1. For the bedrock sites, we used a smaller value than previously suggested for rock formations in Greece (Margaris and Boore 1998) using judgement based on our experience for κ estimates from bedrock sites in the broader

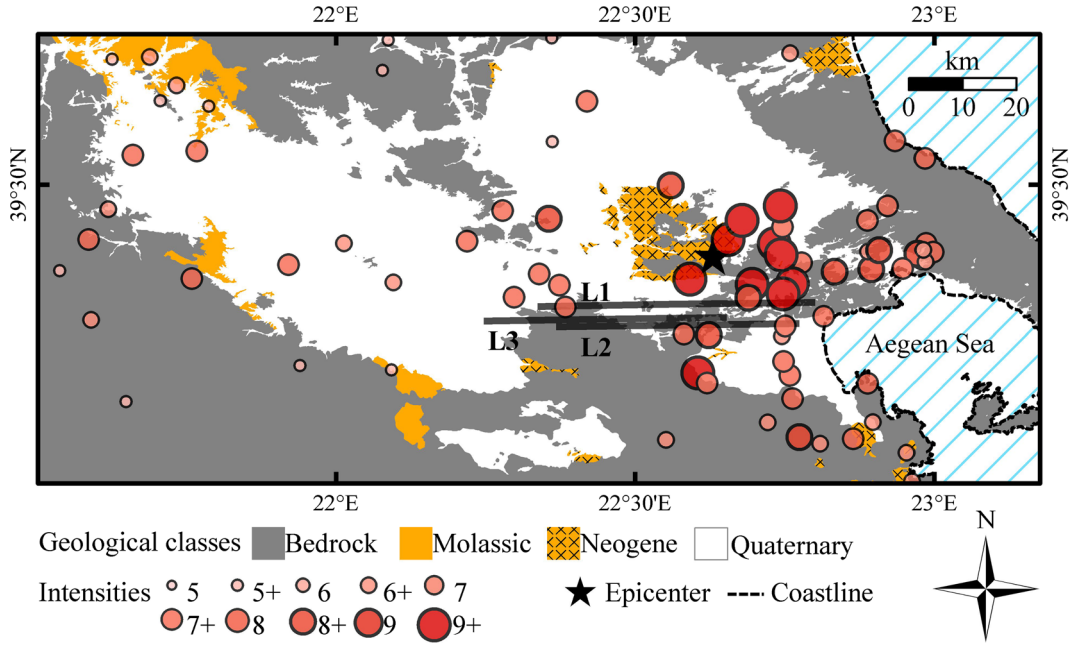

Fig. 3 Observed macroseismic intensities (Modified Mercalli scale), catalogue epicentre of the $M = 6.8$, 1957 Velestino earthquake, and main geological formation classes within the broader Thessaly basin area. The three candidate locations for the upper Farsala fault edge (L1–L3) examined in the present study for the 1957 event are also presented

Aegean area. Table 2 summarises all the parameters of the model adopted in the simulations.

The expected synthetic seismograms were initially simulated without considering the local site-effects (all formations were considered as basement rocks, class 1, with no site amplifications). Following this step, the calculated PGA and PGV values were corrected for site-effects using the constant amplification factors of the GMPE proposed for the Greek area by Skarlatoudis et al. (2003, 2007). For this estimation it was assumed that Bedrock, Molassic/Neogene, and Quaternary/Plio-Pleistocene sediments corresponded to NEHRP soil categories A/B, C and D, respectively, as these were also considered by Skarlatoudis et al. (2003, 2007). Moreover, an additional simulation was performed, assuming the generic spectral amplifications factors proposed for Greece by Klimis et al. (1999), for site classes C and D.

The final step for generating the synthetic macroseismic maps involves the estimation of the expected

Table 1 High-frequency attenuation parameter κ and NEHRP classification, adopted for each geological soil class in the simulations

Geological class	NEHRP class	κ	Reference
1	A/B	0.015	Adopted after tests
2	C	0.044	Klimis et al. (1999)
3	C	0.044	Klimis et al. (1999)
4	D	0.066	Klimis et al. (1999)

Table 2 Parameters of the preferred model used for the strong-motion simulations of the $M = 7.0$, 1954 Sofades earthquake

Strike	271°
Dip	47°
L	44 km
w	18 km
Top-fault depth	1 km
Sub-faults	7x3
ΔL	6.286 km
Δw	6 km
M	7.0
Stress parameter	70 bars
Vrup	0.8
β	3.4 km/s
ρ	2.7 gr/cm^3
κ	(as in Table 1)

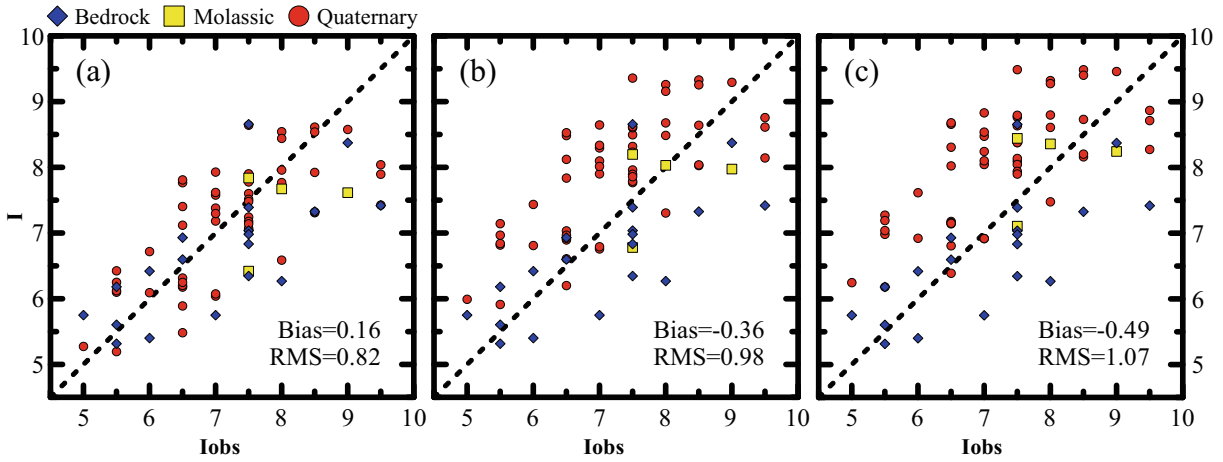

Fig. 4 Comparison of modelled, I, against observed, Iobs, macroseismic intensities for Sofades fault location 1 scenario (see Fig. 2). **a** No site-effects. **b** With the constant site-effect amplification factors of Skarlatoudis et al. (2003, 2007). **c** With the generic spectral site-effect amplifications proposed by Klimis et al. (1999)

macroseismic intensities from the synthetic stochastic seismograms. We have adopted a simple approach, where the PGA and PGV values from the synthetic waveforms were converted to macroseismic intensities (Modified Mercalli scale, I_{MM}, as adapted in Greece). To perform the conversion, we employed the most recently developed approach by Tselentis and Danciu (2008) for the Greek area and the corresponding conversion (4) and (5):

$$I_{MM} = -0.946 + 3.563 * log_{10} PGA \quad (4)$$

$$I_{MM} = 3.3 + 3.358 * log_{10} PGV \quad (5)$$

as they are closer to the average of all previous relations published for the area of Greece (Theodulidis and Papazachos 1992; Koliopoulos et al. 1998).

2.2 Fault location optimisation and site-effect assessment

Initially, we adopted the fault location proposed by Papazachos et al. (2001), depicted as L1 in Fig. 2. The results of this initial simulation, presented in Fig. 4, showed significant deviations between observed (Iobs) and synthetic (I) intensities. These differences were observed both without site amplifications, as well as when using the constant

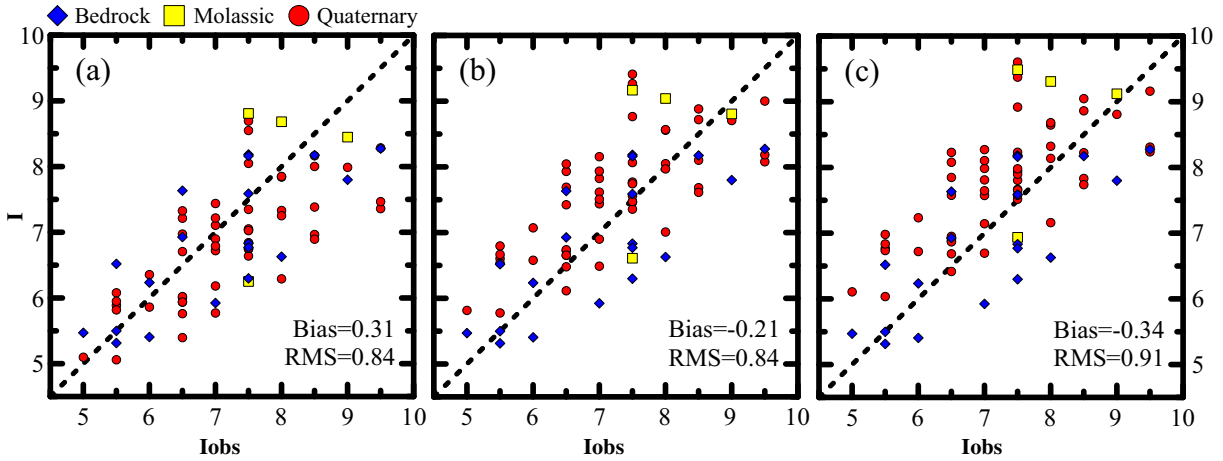

Fig. 5 Same as Fig. 4, for the second fault location simulation (L2 in Fig. 2)

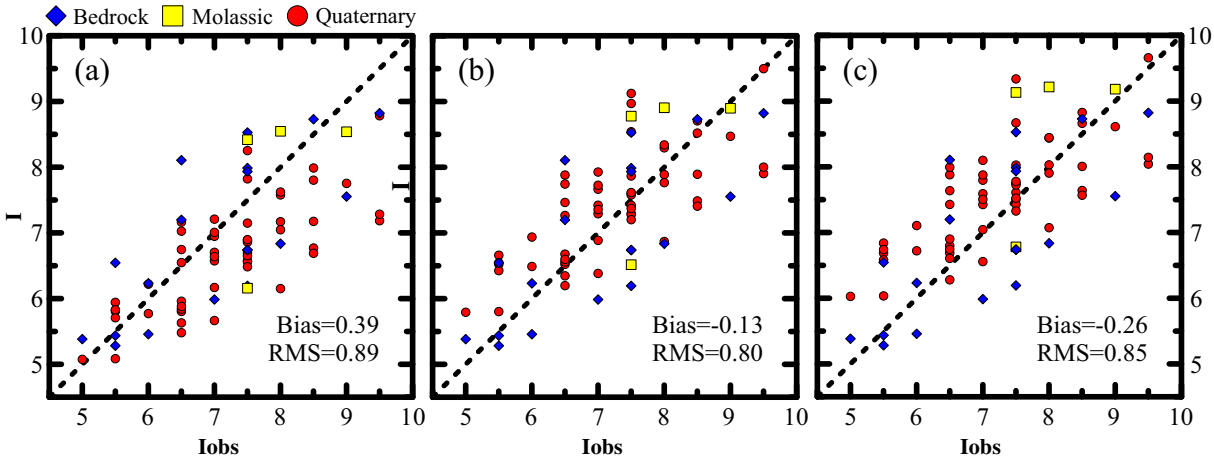

Fig. 6 Same as Fig. 4, for the third fault location examined (L3 in Fig. 2)

site amplification factors proposed by Skarlatoudis et al. (2003, 2007), and the generic spectral amplifications suggested by Klimis et al. (1999). In general, the results show that the modelled intensities for bedrock sites (diamonds in Fig. 4) are lower than the observed intensities. The opposite is observed for soft soil sites, with synthetic macroseismic intensities (no site-effect amplification, Fig. 4a) showing much larger values than the observed ones. This pattern completely contradicts the usual pattern observed for soft soil sites, which are expected to exhibit significantly higher site amplifications. Due to this discrepancy, the bias and RMS of the fit between synthetic and observed macroseismic data became larger when also using site-effect amplifications (−0.49/1.07 intensity bias/RMS for the Klimis et al. (1999) site effects instead of 0.16/0.82 for the case of no site-effects, see also Fig. 4b, c).

In order to explain this discrepancy, it is clear that any simulation scenario would require a reduction of the synthetic macroseismic intensities for the soft soil (essentially Quaternary/Plio-Pleistocene) sites, and an increase for the bedrock sites. This pattern can be partly fulfilled if the fault's upper edge would be located to the south of the initial location examined, being in better agreement with the mapped active faults of the southern Thessaly fault zone (Mountrakis et al. 1993), as these are presented in Fig. 2. For this reason, two additional possible fault locations were considered, depicted as L2 and L3 in Fig. 2.

As Fig. 5 indicates, simulations using the second fault location (L2 in Fig. 2) resulted in slightly smaller deviations between observed and synthetic macroseismic intensities. The third fault location examined (L3 in Fig. 2), which was constrained by the observed surface ruptures and neotectonic faulting of the southern Thessaly basin (Papastamatiou and Mouyaris 1986; Caputo and Pavlides 1993; Mountrakis et al. 1993), also shown in Fig. 2) led to the best results, as is presented in Fig. 6. Figure 6a shows that synthetic and macroseismic intensities for bedrock correlate well when no site amplifications are considered. This correlation verifies our assumption, which is in agreement with the available neotectonic information for the optimal fault location. However, the

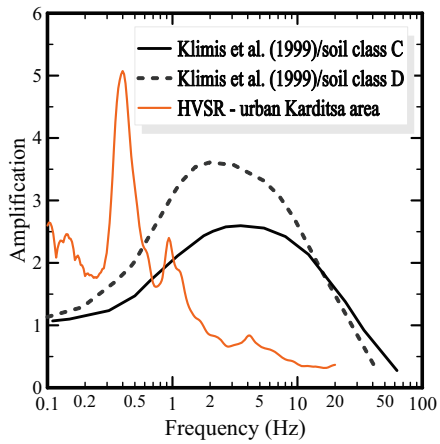

Fig. 7 Comparison of the spectral amplifications proposed by Klimis et al. (1999) for soil classes C and D against the typical HVSR variation with frequency as measured within the urban Karditsa area

soil sites (mostly Quaternary/Plio-Pleistocene sites, class D) show significantly higher observed intensities when no site amplifications are considered for the stochastic simulation results, as expected due to the presence of significant site amplification effects for class D formations. The optimal results have been obtained for the third fault location (L3 in Fig. 2), using the constant amplification factors for PGA and PGV proposed by Skarlatoudis et al. (2003, 2007) for the broader Aegean area. Macroseismic intensities for both bedrock and Quaternary formation sites show a very good correlation between predicted and observed intensities (see Fig. 6b).

It should be noticed that while the overall intensity data modelling improvement is small, it is quite significant. For example for the selected (optimal) fault position (L3), the introduction of site-effects through the local geology index results in smaller intensity bias (−0.13 instead of 0.39 intensity units) and RMS (0.8 instead of 0.89), corresponding to ∼20 % variance reduction between synthetic and observed intensities. While this reduction is not very large, it is clearly statistically significant, as it arises from the introduction of a single site-effect factor. Moreover, recent results for the area of Greece (Stewart et al. 2014) justify the use of geological proxies as site-effects indica-

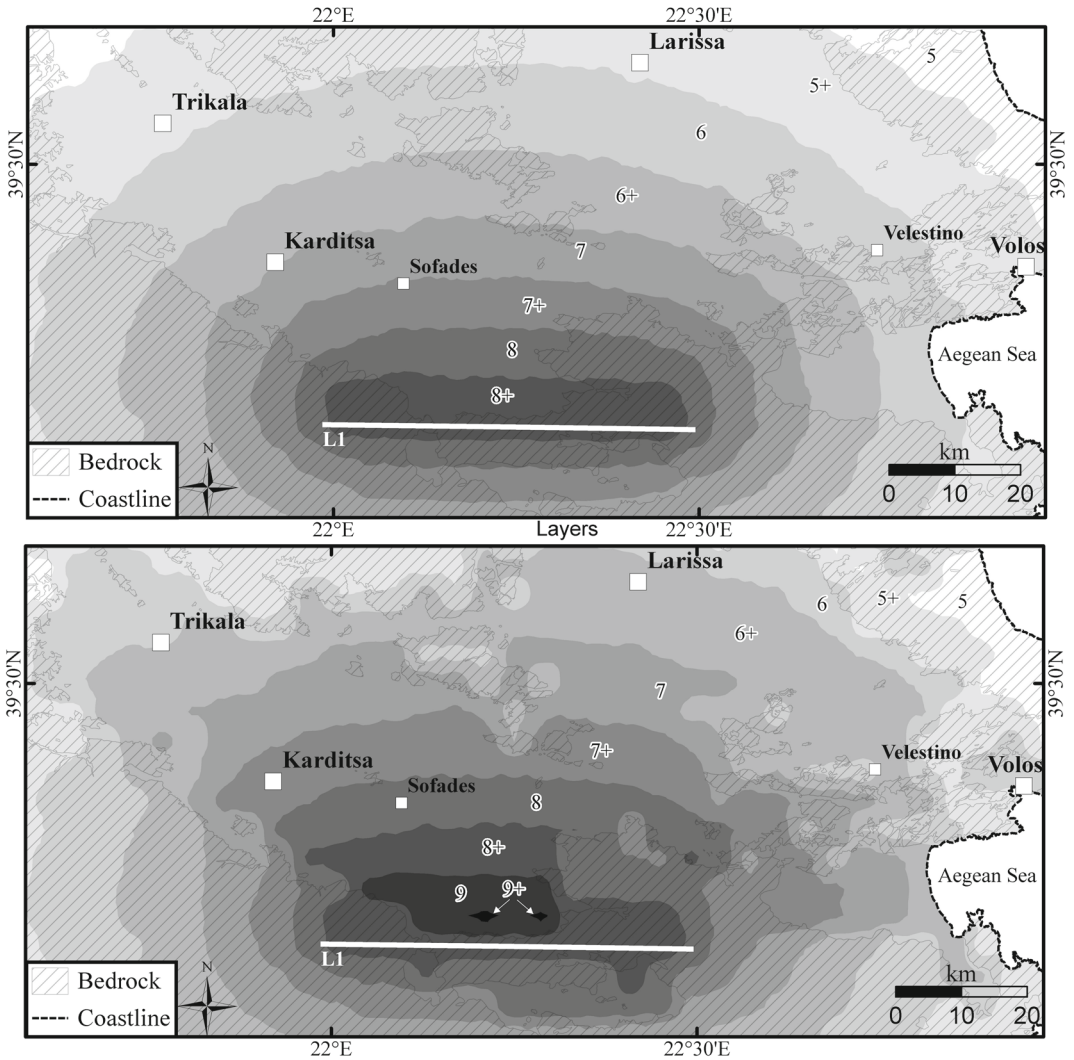

Fig. 8 Estimated macroseismic intensities distribution for the $M = 7.0$, 1954 Sofades event, considering the optimal fault location 3 (see Fig. 2), without the use of site amplifications (*upper figure*) and with the use of the constant PGA/PGV site-effect amplification factors of Skarlatoudis et al. (2003, 2007) (*lower figure*)

tors, showing excellent correlation with traditional site-effect controlling quantities such as V_{s30}.

An interesting feature is that the simulations which were performed using the spectral amplification factors proposed by Klimis et al. (1999) have led to a systematic overestimation of macroseismic intensities for these mainly Quaternary formation sites (Fig. 6c), especially for the central Thessaly basin part. Selected HVSR measurements which were performed in the southern Thessaly basin showed that the recovered resonance frequencies for the central section of the basin (Karditsa area) exhibit very low values (∼0.4 Hz, as shown in Fig. 7), probably due to the significant thickness of the Quaternary deposits. This low-frequency amplification is very different than the corresponding typical (generic) amplification factors proposed by Klimis et al. (1999) for NEHRP class D formations. This discrepancy can be considered as the main reason for the observed bias and resulting macroseismic intensity overestimation.

In order to a posteriori assess the effect of the performed modelling for the broader Thessaly area, we have adopted the final modelling parameters (Table 2, L3, constant amplification factors for soil formations, etc.) and performed computations for a grid of target points with 4 km spacing, in order to estimate the expected damage distribution of the 1954 event, in terms of macroseismic intensities, throughout the whole study area. The final damage distribution maps (with and without using site amplification) are presented in Fig. 8. The results include the effect of the fault geometry, as well as local geology on the expected (and observed) seismic motions. For example, significant modifications of the damage pattern are observed due to the presence of local site-effects, while the hanging-wall area is exhibiting higher seismic motion levels, which are further enhanced for the largest part of the southwestern Quaternary Thessaly basin, due to local site effects.

3 Simulation of the 1957 Velestino earthquake

The collected macroseismic data for the M = 6.8, 1957 Velestino event, included observed intensities (I_{MM}), ranging from 5+ to 9+, for 79 settlements (32 bedrock sites, 3 Neogene sediments sites and 44 Quaternary sediments sites). Table 3 summarises all the parameters adopted for the simulations of the 1957 Velestino event seismic motions. The depth of the upper edge of the fault was also set to 1 km, relatively close to the surface, as existing information suggested the presence of sparse surface fissures/breaks for this event. More specifically, a post-event field survey (Papastamatiou 1957) showed mainly the presence of limited surface fissures (∼500–1000 m), while additional surface deformation effects have not been confirmed (Ambraseys and Jackson 1990). Similar to the 1954 Sofades event, slightly larger depths of 2 and 3 km were also tested for the upper fault edge but no significant differences were observed.

Table 3 Parameters of the preferred model used for strong-motion simulations of the M = 6.8, 1957 Velestino earthquake

Strike	269°
Dip	47°
L	40 km
w	16 km
Top-fault depth	1 km
Sub-faults	8x3
ΔL	5 km
Δw	5.33 km
M	6.9
Stress parameter	70 bars
Vrup	0.8
β	3.4 km/s
ρ	2.7 gr/cm^3
κ	(as in Table 1)

It is evident that the consequences of the foreshock and the mainshock (M = 6.5 and M = 6.8, respectively) cannot be practically distinguished. Although some efforts have been made to discriminate mixed macroseismic effects, especially in the case of aftershocks following a damaging earthquake (e.g. Ferrari et al. 1995; Vannucci et al. 1999), we essentially have a quite comparable foreshock occurring shortly before the mainshock, hence the adopted simulation methodology should not be appropriate for such a case. However, reckoning that this is a typical case with macroseismic and limited seismological data availability, we considered useful to attempt to simulate the 1957 event seismic motions, as if it was a historical earthquake without any information on the detailed features of its foreshock or aftershock sequence (i.e. presence of a strong preshock).

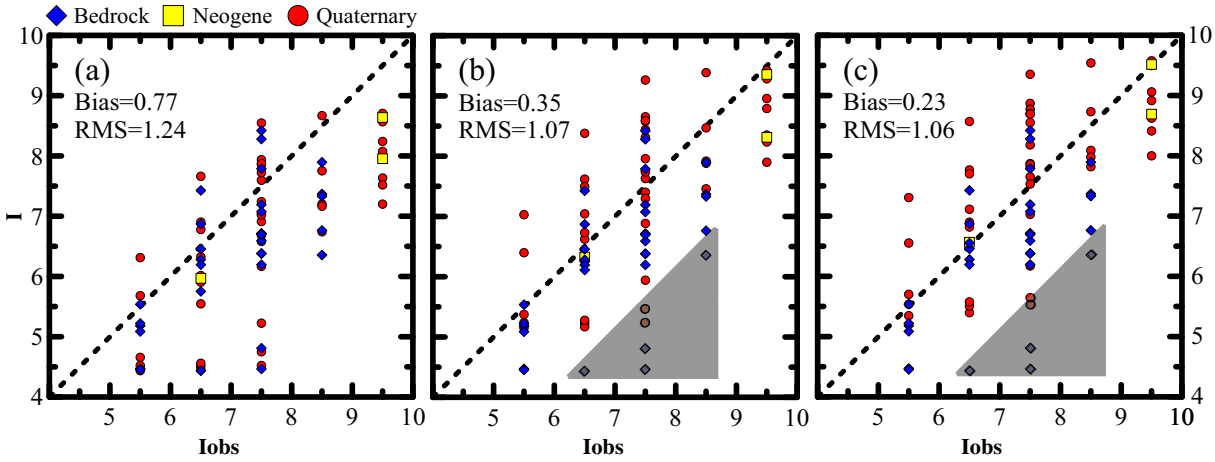

Fig. 9 Comparison of modelled, I, against observed, Iobs, macroseismic intensities for Farsala fault location 1 scenario (see Fig. 3), with a uni-directional rupture and a larger fault length. **a** No site-effects. **b** With the constant site-effect amplification factors of Skarlatoudis et al. (2003, 2007). **c** With the generic spectral site-effect amplifications proposed by Klimis et al. (1999)

As in the 1954 Sofades earthquake simulation, we initially adopted the original fault location proposed by Papazachos et al. (2001). This location was revised through a trial-and-error approach, and two additional fault locations, to the south of the original one, were also tested (L2 and L3 in Fig. 3), compatible with the active faulting of the southern Thessaly presented in Fig. 2. A random rupture scenario was also considered in this case for all examined simulations. However, in all cases, simulations using the examined fault locations resulted in synthetic intensities significantly different from the observed ones, throughout the whole Thessaly area. In general, the calculated (synthetic) intensities where systematically smaller than the observed ones, possibly a result of the combined effect of the mainshock and its strong foreshock on the observed damage pattern.

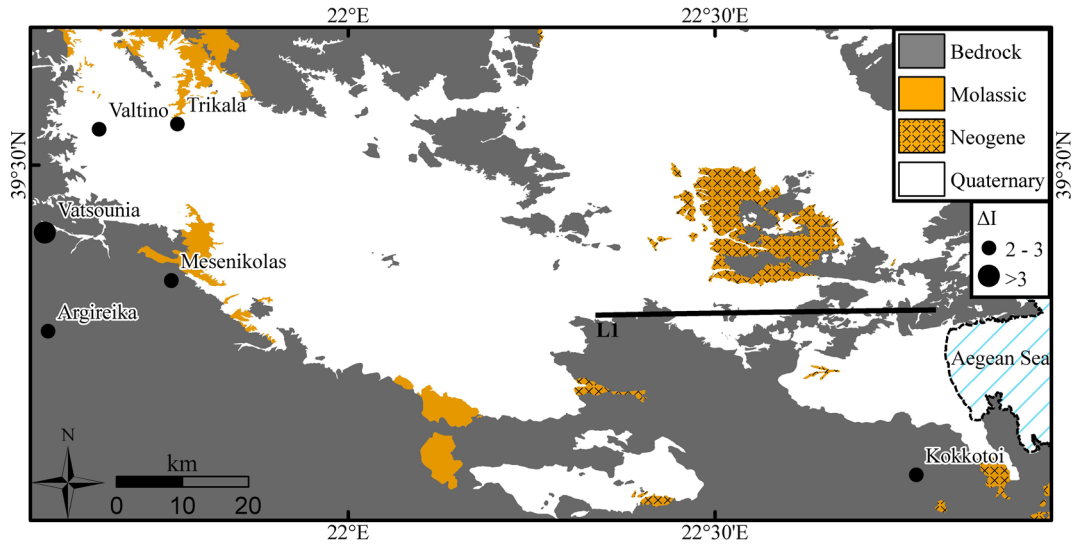

Fig. 10 Sites for which significant bias ($\Delta I \geq 2$) is found between observed (Iobs) and synthetic (I) macroseismic intensties for the 1957 Velestino earthquake

In order to handle this problem, additional configurations were examined, where the rupture length was slightly increased, in order to produce larger synthetic intensities. Moreover, scenarios involving directive rupture were also considered. It should be noted that the observed macroseismic data (Fig. 3) exhibited much larger intensities along the eastern side of the fault (I_{MM} ~8+ to 9+), in comparison to its western section (I_{MM} ~7+), indicating the presence of strong directional rupture phenomena (West-to-East rupture propagation). After these modifications, the only scenario that was sufficiently approximating the observed intensity distribution corresponded to the original Farsala fault location (L1 in Fig. 3), however with a larger length (increased by 5 km towards the east) and an eastwards rupture directivity with V_{rup} = 0.8. This length corresponds to a slightly larger moment magnitude event (M = 6.9), which was expected since additional effects of the large (M = 6.5) foreshock could not be taken into account in the simulations in a systematic manner.

The results of the preferred simulation scenario are presented in Fig. 9, where a good correlation between observed and synthetic macroseismic

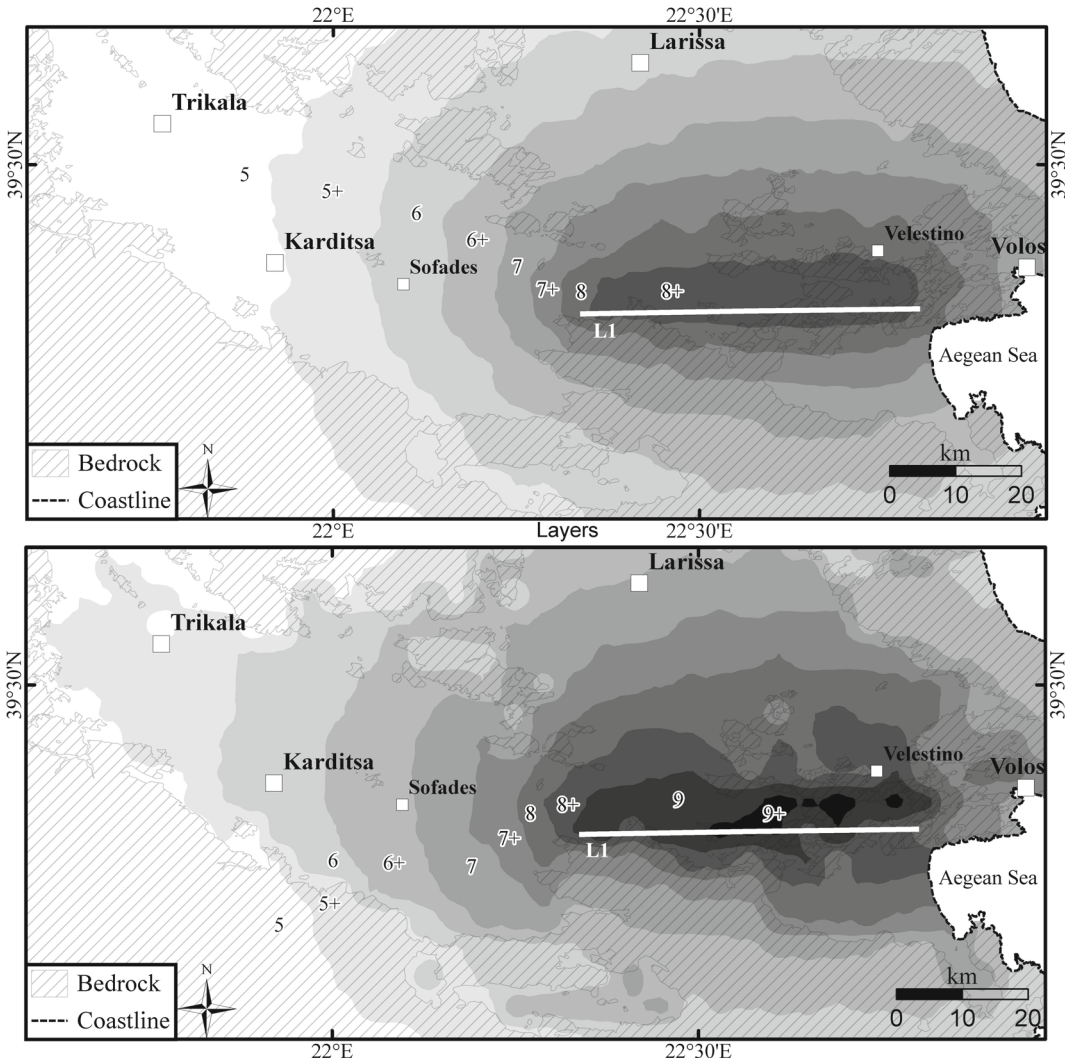

Fig. 11 Estimated macroseismic intensities distribution for the M = 6.8, 1957 Velestino event, considering the optimal fault location 1 (see Fig. 3) with a larger fault length of 40 km, without the use of site amplifications (*upper figure*) and with the use of the constant PGA/PGV site-effect amplification factors of Skarlatoudis et al. (2003, 2007) (*lower figure*)

intensities is noticed for most sites. However, there are six sites (highlighted by a grey triangle in the comparisons presented in Fig. 9b, c) for which simulations significantly underestimate the observed macroseismic intensities, with differences larger than two intensity units. As can be seen in Fig. 10, almost all of these sites are clustered in an area located at the western part of Thessaly, at a distance of approximately 60–80 km from the fault, along its strike. This pattern suggests that the increased observed intensities may be due to specific wave propagation phenomena, such as complex source radiation combined with critical reflections from the Moho (or other intercrustal discontinuities) toward this part of the Thessaly basin, or simply the fact that we are modelling a complex event with a simple uni-directional rupture. Such specific source-rupture/wave-propagation phenomena cannot be simulated using the available information or the adopted stochastic simulation modelling. This suggests that the proposed methodology cannot fully replace detailed wave propagation models. No obvious explanation exists for the underestimation of macroseismic intensity regarding the village of Kokkotoi (eastern Thessaly, see Fig. 10). This is probably a case of typical overestimation of the assigned intensity value, considering that all other intensity values in the vicinity of this site do not exhibit similar bias. An additional reason for the local underestimation of macroseismic intensities is that some of the examined sites are located upon flysch formations (classified as Bedrock, class 1), which, in this case, may locally behave as more loose, susceptible to amplification formations, due to the local geological conditions (e.g. presence of a significant weathered siltstone layer, etc.). It should be noted that the bias and RMS are significantly improved if we exclude these divergent values from the computations. More specifically, the original bias and RMS (Fig. 9b) are reduced to 0.18 and 0.87, respectively, while the ones presented in Fig. 9c are also reduced to 0.06 and 0.84.

The final intensity distribution maps (with and without using site amplification) are presented in Fig. 11. While the constant site-effect amplification factors of Skarlatoudis et al. (2003, 2007) were used also for this case, similar to the 1954 Sofades event simulation, the generic spectral amplification factors of Klimis et al. (1999) show a similar (if not slightly better) performance. This pattern change is

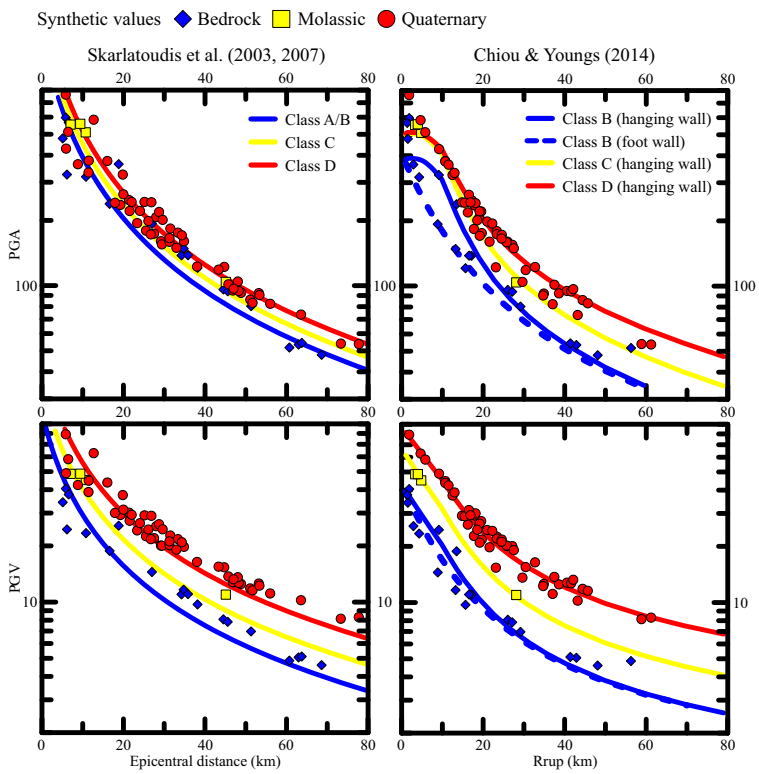

Fig. 12 Comparison of the synthetic PGA (*top figures*) and PGV (*bottom figures*) values obtained for the final 1954 Sofades simulations, against the empirical predictive relations of Skarlatoudis et al. (2003, 2007) for Greece (*left figures*) and of Chiou and Youngs (2014) based on the NGA-West2 PEER world database (*right figures*)

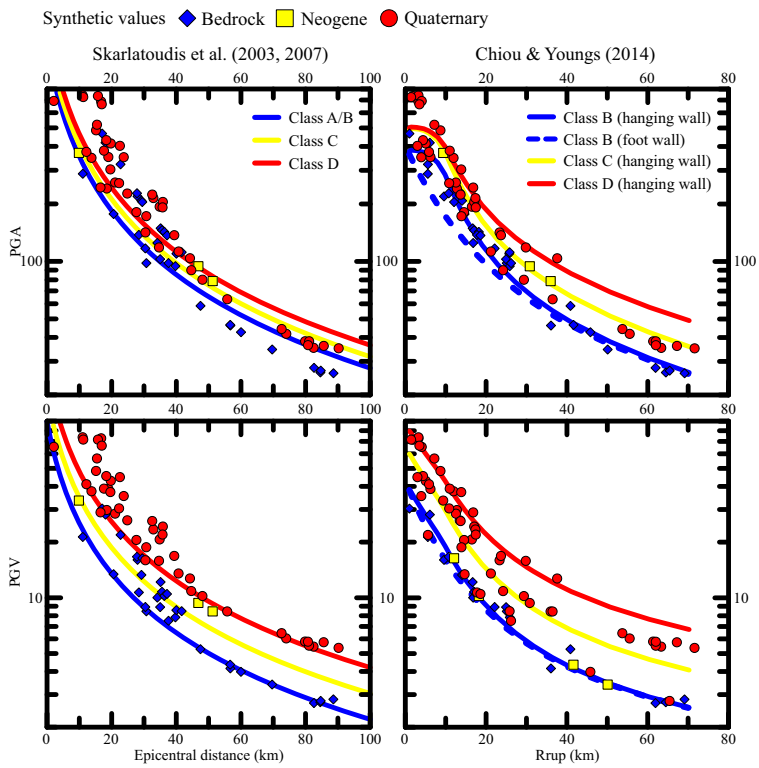

Fig. 13 Comparison of the synthetic PGA (*top figures*) and PGV (*bottom figures*) values obtained for the final 1957 Velestino simulations, against the empirical predictive relations of Skarlatoudis et al. (2003, 2007) for Greece (*left figures*) and of Chiou and Youngs (2014) based on the NGA-West2 PEER world database (*right figures*)

compatible with the general geological setting, since the southeastern part of the Thessaly basin exhibits smaller thicknesses for Quaternary formations, hence the discrepancy observed in Fig. 7 is expected to be less pronounced or even not present.

4 Conclusions

The results obtained in the present study show that the simulation of the rupture of historical earthquakes can be performed by employing macroseismic data and appropriate simulation tools, such as stochastic simulation algorithms (e.g. EXSIM), and by applying appropriate relations converting PGA and PGV values (from synthetic waveforms) to macroseismic intensities, I_{MM} (e.g. Tselentis and Danciu 2008). The simulations also suggest that the use of calibrating equations for fault dimensions assessment (e.g. Papazachos et al. 2004; Papazachos et al. 2006), can lead to realistic results, even for historical earthquakes. This agreement is also confirmed by the comparison of the synthetic PGA and PGV values (obtained from the final simulation scenarios of both examined events) with the empirical predictive relations of Skarlatoudis et al. (2003, 2007) proposed for the broader Aegean area, as presented in Figs. 12 and 13. A good fit is also observed in the same figures for the Chiou and Youngs (2014) relation, which is based on the recent NGA-West2 world strong-motion database from similarly active seismotectonic environments like the Aegean area. It should be noticed that we employ the R_{rup} (instead of epicentral) distance for the later comparison, presenting equations for the hanging-wall (where most synthetic PGA/PGV values refer), while the foot-wall relation is also presented for bedrock sites for completeness. Similar fits were also obtained for all other NGA2 PEER relations (Abrahamson et al. 2014; Boore et al. 2014; Campbell and Bozorgnia 2014)

From the performed simulations, it can be suggested that the originally proposed locations for the Sofades and Farsala faults, as constrained by the already published information, can be updated on the basis of the available macroseismic information. Using the simulated macroseismic intensities, especially for sites on bedrock formations which are not affected by site-effects, it was possible to relocate

the Sofades fault towards the southern edge of the southwest Thessaly basin. The proposed location (L3 in Fig. 2) is in very good agreement with the available neotectonic data for the area (e.g. Mountrakis et al. 1993). Moreover, the obtained results confirm the significant effect of local geology on strong seismic motion, showing important differentiation in the ground response of bedrock formations against Quaternary / Plio-Pleistocene sediment sites.

The results obtained in this study have showed that the generic transfer functions proposed by Klimis et al. (1999) for the area of Greece could not realistically describe the observed site-effects, resulting in very high amplifications for the Quaternary/Plio-Pleistocene sediments. This discrepancy is most probably due to the high Quaternary sedimentary thickness of the southern Thessaly basin (several hundred meters), leading to low-frequency amplifications that are not adequately reflected in the generic transfer functions, in agreement with the available H/V information. Contrariwise, the constant amplification factors proposed by Skarlatoudis et al. (2003, 2007) for PGA and PGV resulted in satisfactory simulation results and realistic site amplification estimates.

The simulation for the M = 6.8, 1957 Velestino event was less effective, probably due to the fact that the observed damage distribution was also affected by its strong foreshock. Moreover, the employed spectral and constant site-amplification factors produced identical synthetic damage patterns, with equivalent fit to the original damage distribution. Despite this being a complex event, we were still able to model it using a single event damage distribution, by involving a fault with larger dimensions. A uni-directional rupture distribution has been employed in order to explain the observed spatial asymmetry of the damage distribution. This observation suggests that it is still possible to model efficiently even complex historical events using their macroseismic data, without introducing significant bias in the final model estimates (e.g. moment magnitude, etc.).

Acknowledgments The new digitized geological map of the broader Thessaly area used in this study was produced from the digitization of the corresponding 1:50000 geological maps of the Greek Institute of Geology and Mineral Exploration (IGME). We would like to thank George Vargemezis for providing help with the geological maps used. HVSR results for the broader Karditsa area were obtained from HVSR measurements performed within this study. All remaining data used in this work were collected from published sources, referenced in the manuscript. The contribution of Costas Papazachos and Harris Kkallas was partly realised within the 3D-SEGMENTS ARISTEIA project, funded by the EC Social Fund and the Greek Secretariat of Research and Technology.

References

Abrahamson NA, Silva WJ, Kamai R (2014) Summary of the ASK14 ground motion relation for active crustal regions. Earthq Spectra 30:1025–1055

Ambraseys NN, Jackson JA (1990) Seismicity and associated strain of central Greece between 1890 and 1988. Geophys J Int 101:663–708

Atkinson GM, Boore DM (1995) Ground-motion relations for eastern North America. Bull Seism Soc Am 85:17–30

Beresnev IA, Atkinson GM (1999) Generic finite-fault model for ground-motion prediction in eastern North America. Bull Seism Soc Am 89:608–625

Boore DM (1983) Stochastic simulation of high-frequency ground motions based on seismological models of the radiated spectra. Bull Seism Soc Am 73:1865–1894

Boore DM (2009) Comparing stochastic point-source and finite-source ground-motion simulations: SMSIM and EXSIM,Bull Seism Soc Am 99(6):3202–3216

Boore DM, Atkinson GM (1987) Stochastic prediction of ground motion and spectral response parameters at hard-rock sites in eastern north America. Bull Seism Soc Am 77:440–467

Boore DM, Joyner WB (1997) Site amplifications for generic rock sites. Bull Seism Soc Am 87:327–341

Boore DM, Stewart JP, Seyhan E, Atkinson GM (2014) NGA-West2 equations for predicting PGA, PGV, and 5 % damped PSA for shallow crustal earthquakes. Earthq Spectra 30:1057–1085

Campbell KW, Bozorgnia Y (2014) NGA-West2 ground motion model for the average horizontal components of PGA, PGV, and 5 % damped linear acceleration response spectra. Earthq Spectra 30:1087–1115

Caputo R, Pavlides S (1993) Late cainozoic geodynamic evolution of thessaly and surroundings (central-northern Greece). Tectonophysics 223(3):339–362

Chiou BS, Youngs RR (2014) Update of the Chiou and Youngs NGA model for the average horizontal component of peak ground motion and response spectra. Earthq Spectra 30:1117–1153

Ferrari G, Gasperini P, Guidoboni E (1995) Macroseismic intensity evaluation with the fuzzy sets logic. Annali di Geofisica 38(5-6):811–826

Klimis NS, Margaris BN, Koliopoulos PK (1999) Site-dependent amplification functions and response spectra in Greece. J Earthq Eng 3(02):237–270

Koliopoulos PK, Margaris BN, Klimis NS (1998) Duration and energy characteristics of Greek strong motion records. J Earthq Eng 2(3):391–417

Lekkas E (1987) Geological structure and geodynamic evolution of the Koziakas range (western Thessaly) (in Greek), PhD thesis, Department of Geology, National and Kapodestrian University of Athens

Margaris BN, Boore DM (1998) Determination of $\Delta\sigma$ and $\kappa 0$ from response spectra of large earthquakes in Greece. Bull Seism Soc Am 88:170182

Motazedian D, Atkinson GM (2005) Stochastic finite-fault modelling based on a dynamic corner frequency. Bull Seism Soc Am 95:991010

Mountrakis D, Kilias A, Pavlides S, Zouros N, Spyropoulos N, Tranos M, Soulakelis N (1993) Field study of the southern Thessaly highly active fault zone. In: Proceedings of the 2nd Congress of the Hellenic Geophysical Union, vol 2, p 603614

Ou GB, Hermann RB (1990) Estimation theory for peak ground motion. Seismol Res Lett 61(2):99–107

Panagiotopoulos DG, Papazachos CB (2008) Application of modern methods for assessing the seismicity of Karditsa. In: Proceedings of the 1st development conference of Karditsa

Papastamatiou I (1957) The earthquake of Velestino of 8 March 1957, Report Inst. Geologias & Erevnon Ypedaphus, p 11, Athens

Papastamatiou D, Mouyaris N (1986) The earthquake of April 30, 1954, in Sophades (central Greece). Geophys J R astr Soc 87:885–895

Papazachos BC, Papazachou C (2002) The earthquakes of Greece. Ziti Publ., Thessaloniki

Papazachos BC, Comninakis PE, Drakopoulos JC (1966) Preliminary results of an investigation of crustal structure in southeastern Europe. Bull Seism Soc Am 56(6):1241–1268

Papazachos BC, Hatzidimitriou PM, Karakaisis GF, Papazachos CB, Tsokas GN (1993) Rupture zones and active crustal deformation in southern Thessalia, central Greece. Boll Geof Teor Appl 35:363–374

Papazachos BC, Papaioannou Ch, Papazachos CB, Savvaidis AS (1997) Atlas of isoseismal maps for strong shallow earthquakes in Greece and surrounding area (426bc-1995). Ziti Publ., Thessaloniki

Papazachos BC, Mountrakis DM, Papazachos CB, Tranos MD, Karakaisis GF, Savvaidis AS (2001) The faults which have caused the known major earthquakes in Greece and surrounding region between the 5th century bc and today. In: Proceedings of 2nd National Conference Anti-Seismic Engineering and Technical Seismology, p 1726

Papazachos BC, Scordilis EM, Panagiotopoulos DG, Papazachos CB, Karakaisis GF (2004) Global relations between seismic fault parameters and earthquake moment. Bull Seism Soc Am 36:1482–1489

Papazachos BC, Karakaisis GF, Papazachos CB, Scordilis EM (2006) Perspectives for earthquake prediction in the Mediterranean and contribution of geological observations. In: Robertson AHF, Mountrakis D (eds) Tectonic Development of the Eastern Mediterranean, vol 260. Publ Geol Soc, London, p 689707

Skarlatoudis AA, Papazachos CB, Margaris BN, Theodulidis N, Papaioannou Ch, Kalogeras I, Scordilis EM, Karakostas V (2003) Empirical peak ground motion predictive relations for shallow earthquakes in Greece. Bull Seism Soc Am 93:2591–2603

Skarlatoudis AA, Papazachos CB, Margaris BN, Theodulidis N, Papaioannou Ch, Kalogeras I, Scordilis EM, Karakostas V (2007) Erratum to empirical peak ground motion predictive relations for shallow earthquakes in Greece. Bull Seism Soc Am 97:2219–2221

Stewart JP, Klimis N, Savvaidis A, Theodoulidis N, Zargli E, Athanasopoulos G, Pelekis P, Mylonakis G, Margaris B (2014) Compilation of a local Vs profile database and its application for inference of Vs30 from geologic- and terrain-based proxies. Bull Seism Soc Am 104:2287–2841

Theodulidis NP, Papazachos BC (1992) Dependence of strong ground motion on magnitude-distance, site geology and macroseismic intensity for shallow earthquakes in Greece: I, peak horizontal acceleration, velocity and displacement. Soil Dyn Earthq Eng 11(7):387–402

Toro GR, McGuire RK (1987) An investigation into earthquake ground motion characteristics in eastern north America. Bull Seism Soc Am 77(2):468–489

Tselentis GA, Danciu L (2008) Empirical relationships between modified Mercalli intensity and engineering ground-motion parameters in Greece. Bull Seism Soc Am 98(4):1863–1875

Vannucci G, Gasperini P, Ferrari G, Guidoboni E (1999) Encoding and computer analysis of macroseismic effects. Phys and Chem of the Earth 24:505–510

Zonno G, Oliveira CS, Ferreira MA, Musacchio G, Meroni F, Mota-de-Sa F, Neves F (2010) Assessing seismic damage through stochastic simulation of ground shaking: the case of the 1998 Faial earthquake (Azores Islands). Surv Geophys 31:361–381